Int. J. Multiphase Flow, Vol. 2, pp. 379–395. Pergamon/Elsevier, 1976. Printed in Great Britain.

INSTABILITY WAVES AND THE ORIGIN OF BUBBLES IN FLUIDIZED BEDS

PART 1: EXPERIMENTS

M. M. EL-KAISSY and G. M. HOMSY

Department of Chemical Engineering, Stanford University, Stanford, CA 94305, U.S.A.

(*Received* 11 *June* 1975)

Abstract—Statistically significant measurements of the propagation properties of instability waves in a two-dimensional liquid fluidized bed are reported. Visual and quantitave measurements show that although the waves experience an initially exponential growth in amplitude, the ultimate state of motion exhibited is that of the complicated formation and destruction of cylindrical bubble-like structures. Expected values of their amplitude, frequency, and velocity are measured, and preliminary scaling laws are proposed. The implication is that bubbles in gas-fluidized beds are a result of the same instability of the state of uniform fluidization.

1. INTRODUCTION

One of the most striking phenomena of fluidization is the occurrence of particle-free regions known as "bubbles". A great deal is known about the dynamics of a single isolated bubble in gas-fluidized beds; this body of knowledge recently been reviewed by Rowe (1971). More recent work has focused on bubble distribution in freely-bubbling beds, Werther & Molerus (1973), and bubble stability, Clift & Grace (1972). In spite of these advances, the origin of bubbles has, until recently, been poorly understood. It has been known empirically for some time that the ratio of fluid to solid densities is important in determining if a system will bubble, that polydisperse systems bubble less pronouncedly than monodisperse systems, and that beds of very fine particles will not bubble until conditions removed from minimum fluidizations are reached. Finally, a transition criterion due to Wilhelm & Kwauk (1949) based upon a Froude number seems to hold some merit, but no satisfying explanation has yet emerged as to why this should be so. Thus to date, the origin of bubbles has been unexplained.

A group of workers promote the idea that the bubbles are generated at orifices of typical multiorifice distributor whose structure has a definite effect on the quality of fluidization (see e.g. Zenz, 1971). This view, while possibly correct, does not explain the occurrence of bubbles in spite of extensive effort to assure uniform distribution.

Hiby (1967) proposed a simple analysis of the quasi-periodic oscillations of particles in shallow gas fluidized beds, assumed to be remotely connected to the triggering mechanism for the periodic formation of gas bubbles in deep beds. This phenomena has been further studied by Jones & Pyle (1971), and recently Verloop & Heertjes (1974) have postulated that a loss of coherence in the particle phase is responsible for bubble birth. While plausible, there does not exist, to our knowledge, experimental evidence with which to judge the correctness of the theory.

Jackson (1963), and later Anderson & Jackson (1968) considered the formation of bubbles to be interrelated to an instability of the state of uniform fluidization. Analysis showed that the state was always unstable to small perturbations and, even more strikingly, they were able to demonstrate that the growth rate of the disturbance in gas–solid systems was an order of magnitude greater than that for liquid–solid systems. Surprisingly, there seems to have been very early experimental evidence for this point of view which was, for the most part, ignored.

In a series of papers, Hasset (1961a, 1961b) reported that upon close observation of liquid fluidized beds, which were generally believed to fluidize in a uniform manner, nonhomogeneities were apparent. It was also demonstrated by many investigators (Lawson & Hasset 1967, Jackson 1963, Anderson & Jackson 1969) that such narrow band, horizontal, travelling-wave disturbances were not the consequence of any possible fluid maldistribution but are rather valid instability

phenomena of a fluidized suspension. Such disturbances can be described analytically (at least in the early stages of their development) by linear stability theory as presented by Jackson (1963) and Anderson & Jackson (1968).

Modeling multiparticle systems is recognized as a very difficult task. Several different approaches have been proposed for the equations of motion of fluidized beds. Two familiar physical situations in fluidization have been given attention in order to test the validity of the proposed equations. These are the motion of an isolated bubble in a fluidized bed and the propagation of small disturbances about the state of uniform fluidization. It is also well known that in spite of the extensive experimental data available on the motion of an isolated bubble in a fluidized bed, a test of the proposed equations based on this physical phenomenon involves a large number of approximations and the neglect of many terms so that the final answer obtained is only indicative of the overall validity of the momentum and mass balances (see e.g. Jackson 1971).

The study of propagation properties of small disturbances about the state of uniform fluidization appears to be a more decisive test of the modeling equations since in such a study all terms except those which are nonlinear in disturbance amplitude are retained. The effect of each term on the behavior of the system under study can thus be investigated systematically.

To this end, the experimental program described below had as one of its objectives the gathering of high quality data describing the propagation properties of the traveling wave disturbances. The only other study with similar objectives was by Anderson & Jackson (1969), but was dependent on visual analysis of data. A detailed discussion of their results is given by El-Kaissy (1975); it suffices here to say that the quantitative results of the Anderson & Jackson (1969) study are extremely suspect.

A dual objective of this investigation derives from the fact that the origin of "bubbles", typically observed in gas fluidized beds, remains a mystery and lacks any satisfying explanation at the present time. It was hoped that such a study, in conjunction with theoretical developments described in a later paper, might be able to shed some light on this phenomenon.

The work reported here represents, as far as we are aware, the first quantitative study of the instability wave motion which occurs above minimum fluidization in which adequate data reduction methods were used. In addition to providing measurements of the wave properties, certain visualizations of the disturbances, together with supporting statistical data, demonstrate beyond any doubt that the advanced stages of wave breakup are characterized by nearly cylindrical clusters of low voidage, which are the counterpart of bubbles in gas systems. The apparatus is described in section 2, after which the flow visualizations are described (section 3). The quantitative determination of propagation properties is presented in section 4, and section 5 contains a discussion of the main features of these results. In section 6, we give an overview of the mechanism of growth and breakup of the waves and subsequent formation of bubble clusters.

2. APPARATUS

Experiments were carried out in a Plexiglas column of 2.22×7.62 cm cross-section and 1.22 m high. Figure 1 shows a schematic of the apparatus. A 0.61 m section was placed above the test section to minimize end effects. Particular care was taken to obtain uniform fluid distribution at the base. This was necessary to ensure that the observed disturbances were not the result of maldistribution, but rather a consequence of the physical behavior of the bed. The distributor was composed of a bundle of equally spaced 0.48 cm diameter Plexiglas tubes; the top section was a 10.16 cm deep packed bed of 0.51 cm diameter particles. The bed support was a sintered bronze porous plate. Large pressure drop distributors such as porous plates are desirable since they are known, both experimentally and theoretically (Medlin *et al.* 1974) to reduce the intensity of local vortical motion of particles close to the base of the bed.

Distilled water was used as the fluidizing medium. A 560 W pump was used to circulate the water in a closed loop from a 189.3 l holdup tank through a pair of Dwyer rotameters (Ratemaster

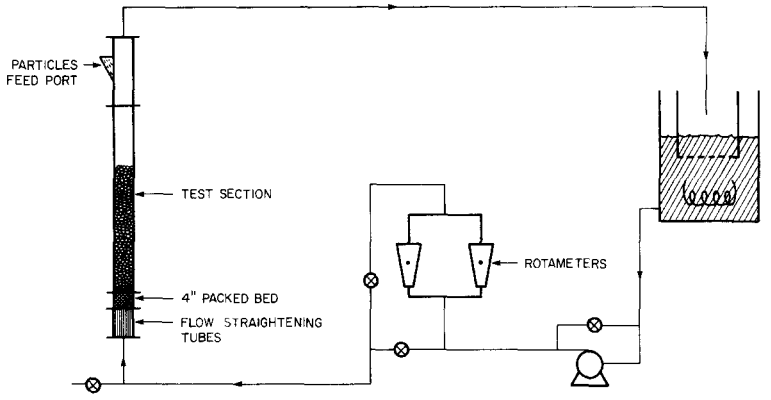

Figure 1. Schematic of the apparatus.

models RMC-141-SSV-PF and RMC-143-SSV-PF). The temperature of the circulating water was measured at two points in the flow system; within the holdup tank and inside the column, just above the test section. A cooling system maintained the fluid temperature at 25 ± 2°C. All piping was 2.54 cm PVC schedule 40.

3. VISUAL OBSERVATIONS

In this section we describe visual observations made of the wave behavior. In the sequel some terms will be encountered that should be given precise definition. By a "coherent wave" we mean a wave that is one-dimensional and spans the width of the column. "Coalescence" denotes the phenomenon of two or more of the wave-like disturbances approaching one another sufficiently close to form a resulting disturbance which may or may not be coherent. The term "turbulent" is used to describe the chaotic, random motion of particles as viewed in a continuum or ensemble sense. In certain flow regimes, the motions appear well ordered (in the continuum sense), and we distinguish these "laminar" states from those in which no discernible order is apparent.

Table 1 gives the properties as well as the size range of the beads under investigation. The experimentally determined values of voidage and velocity at minimum fluidization conditions are included. We also give the ratio of bed thickness to particle diameter for all cases studied. The range of flow rates covered for each bead size is given in table 2.

Extensive flow visualizations were carried out using both 16 mm motion pictures and still photography. The bed was backlit with two 500 W flood lamps, with a diffuser screen placed between the bed and lamps. In this manner, voidage variation of a few tenths of a per cent were visible to the unaided eye, due perhaps to the relatively large index of refraction of these particular beads.

Upon increasing the flow rate slightly above that required for minimum fluidization, horizontal bands of high voidage regions about a centimeter wide appear to propagate up the bed. Depending on the flow rate, they either lose their horizontal structure and seem to become convex, hug one wall, or zig-zag and coalesce with the leading wave. In some cases, the waves

Table 1. Properties of glass beads

Set No.	Code*	Diameter, d_p (mm)	Dominant diameter (mm)	u_{mf} (cm/s)	ϵ_{mf}	Bed depth, D/d_p
A	304 class C (Ballotini No. 5)	0.589–0.417	0.59	0.64	0.35	38
B	203 class C (Ballotini No. 7)	0.833–0.589	0.83	1.09	0.367	27
C	−16+18 mesh class V	1.19 −1.00	1.1	1.90	0.395	20
D	−12+14 mesh class V	1.68 −1·41	1.56	2.75	0.386	15

*Microbeds Division, Cotaphote Corporation, Jackson, Mississippi 39205.

Table 2. Flow conditions for experimental measurements

Set	u (cm/s)	ϵ	u/u_{mf}	Data points (Figures 8–19)
A	0.95	0.401	1.49	○
	1.04	0.422	1.63	□
	1.12	0.427	1.75	△
B	1.49	0.410	1.37	○
	1.68	0.425	1.54	□
	1.86	0.441	1.71	△
C	2.61	0.45	1.37	○
	2.68	0.456	1.41	□
	2.76	0.461	1.45	△
D	3.73	0.441	1.36	○
	4.10	0.459	1.49	□
	4.47	0.473	1.63	△

break up and have no identifiable structure other than generating small "pockets" of high voidage regions, while in other cases coalescence or breakup is followed by a new coherent traveling wave. The upper surface of the bed remains horizontal as waves reach it.

The vertical extent of the planar wave motion becomes smaller with increased flow rate, while coalescence and breakup is more frequent. The range of flow rates in which waves remain coherent over any measurable distance was relatively small (about twice the minimum fluidization velocity). The particles remain stationary in the mean in the regime where coherent waves exist, oscillating about a fixed position as the waves pass. At much higher flow rates turbulent motion occurs and particles wander randomly around the bed. Regions of bubble-like clusters can be clearly seen although the bed is superficially more homogeneous in structure than before.

Figure 2 shows a limited number of such visualizations which illustrate the phenomenon of wave formation, growth, and breakup in clusters. These photographs are for the largest bead size, for which the motions have their highest amplitudes (see section 5). The first photograph (figure 2a) shows the wave structure for a velocity ($u/u_{mf} = 1.36$) for which the planar coherence is evident over approximately 1/3 of the bed. The waves in the lowest section are not easily visible, being of low amplitude, but at least 4 waves are readily discernible. The wave length increases dramatically after loss of coherence. At least one wave is pictured in the process of breaking up.

Figure 2b pictures the same beads at a higher flow rate, $u/u_{mf} = 1.5$. The region of coherence is now confined to a region closer to the distributor. The structure is clearly one of breakup, coalescence, and cluster formation. Little instructive information can be obtained visually in this regime, as the motions must be described statistically (see section 5). However, we do point out at least two events leading to bubble cluster formation.

Figure 2c graphically illustrates the formation of one of these clusters. A wave in the middle of a forward moving wave train is seen to exhibit a buckle or wrap-around instability, resulting in the formation of an approximately circular cluster. From motion picture visualizations, we have observed that such clusters have a higher velocity of propagation than a planar wave, with the obvious result that clusters such as those pictured in figure 2b are extremely short lived. They rise quickly to merge with the wave immediately ahead, which in turn results in a momentary loss of coherence of the motion as a whole.

In conclusion, at low flow rates coherent and horizontal waves persist. As the flow rate is increased a smaller planar region exists close to the distributor, but in higher portions of the bed the waves become convex, zig-zag and coalesce. The resultant structure after coalescence seems to depend on the amplitude of the final disturbance. If this is small enough, another coherent wave will result, while if the amplitude is large, breakup of the waves into small, high-voidage regions or bubble-like clusters occurs.

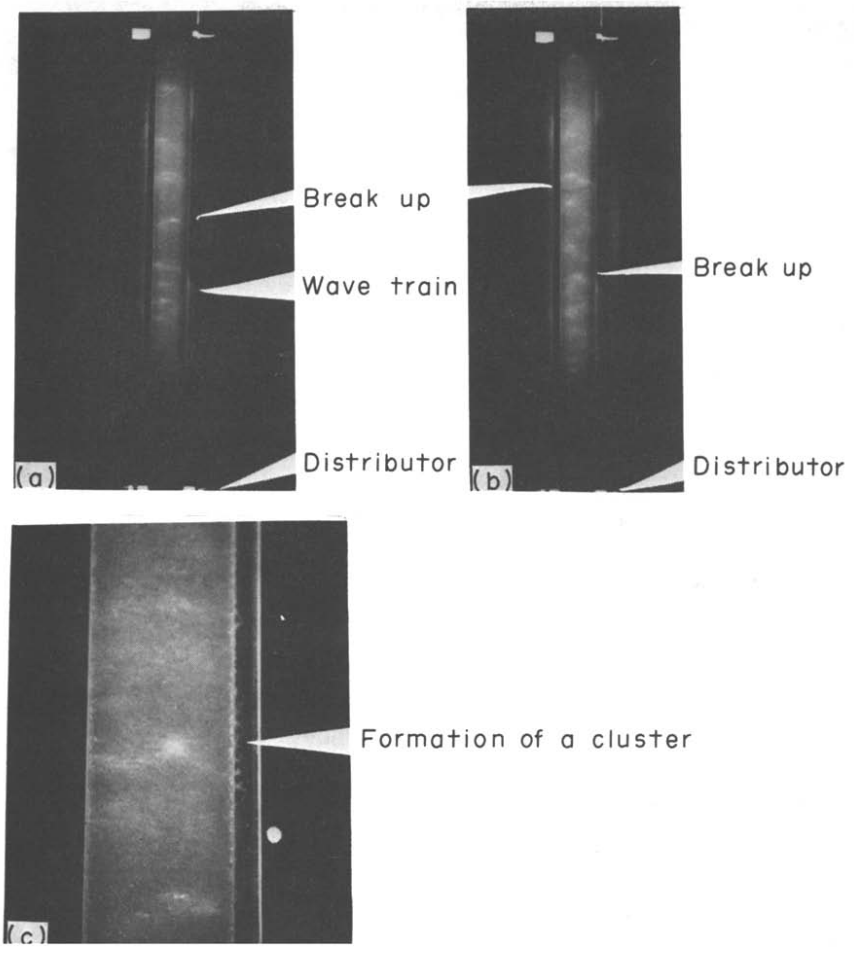

Figure 2. Visualizations of wave structure and break-up.

4. QUANTITATIVE MEASUREMENTS

The main objective of this phase of the experimental program was to gather high quality data suitable for comparison with proposed theoretical models. To accomplish this, automatic data logging and analysis techniques were implemented. The wave-like disturbances of interest are fully characterized by obtaining a statistical measure of the following three quantities: the amplitude, velocity of propagation and frequency distribution. These measurements were made using a light transmission technique. One of the main advantages of this method is that the flow remains undisturbed.

Before describing the photodetection equipment, we indicate that the gross bed behavior was in accord with previous studies. For bubble-free fluidized systems, a widely accepted correlation for bed expansion is that proposed by Richardson & Zaki, cf. Davidson & Harrison (1968),

$$u/u_t = \epsilon^n$$

where u is the superficial fluid velocity, u_t is the terminal velocity of the particles and n is an exponent depending on $Re_t = (u_t d_p/\nu)$ and weakly dependent on the ratio (d_p/D) of particle diameter to bed width. The relations between n and Re_t are given by

$$\begin{aligned}
n &= 4.65 && Re_t < 0.2,\\
n &= 4.35\, Re_t^{-0.03} && 0.2 < Re_t < 1,\\
n &= 4.45\, Re_t^{-0.1} && 1 < Re_t < 500,\\
n &= 2.39 && Re_t > 500.
\end{aligned}$$

The expansion data for each bead size were plotted as u vs ϵ in a log–log plot. The exponent n and u_t were estimated from these plots and compared with those predicted from the above relations and from correlations for terminal velocities of spherical particles. Table 3 summarizes the extrapolated and predicted values of u_t and n. Note the extrapolated u_t do not compare favorable with the predicted u_t due to the large extrapolation made to $\epsilon = 1$. Thus the exponents predicted based on the experimental u_t were not expected to compare favorably with the experimentally obtained n. However, the exponents based on the predicted u_t are in excellent agreement with experimentally obtained values. Such agreement also indicates that the dependence of n on d_p/D is negligible for d_p/D sufficiently large.

The photodection package is composed of three main parts: the light box, the photodiode box and the signal conditioner. A detailed description of each part of the photo-optical package is given by El-Kaissy (1975). Narrow dual beams of light passed through the bed and impinged on photodiodes located opposite the light source. The intensity of light reaching the diode is thus a direct measure of the local voidage. A DC light bulb was used as the light source to avoid introduction of 60 Hz noise into the signal and to avoid any fluctuation in line voltage. The choice of aperture size was critical in obtaining meaningful records. Apertures of 0.64 cm opening were selected by trial and error. The photodiode box was a $6.35 \times 6.35 \times 12.7$ cm brass box in which two photodiodes were precision mounted vertically above each other. The top diode could be moved relative to the lower one. The diodes were optically shielded from one another to prevent any "cross talk" between them. The beam of light passed through a preset aperature into a blackened tunnel before reaching the photodiodes. Again, the aperture was crucial for good data acquisition. Too small a slit width resulted in a resolution of motion of individual beads or groups of beads rather than the measurement of the continuum motion. On the other hand, the slit had to be small enough to allow resolution of the motions on the length scale of the waves. The aperture required to give good experimental traces was again found to be ~ 0.64 cm for all bead sizes investigated. The distance between the diodes was accurately set at 3.5 cm.

The photodiode and light boxes were connected to one another by means of two screw rods which, after positioning, could be tightened firmly. Careful aligment was necessary in order to obtain reproducible results.

Figure 3 shows a flow chart of the data acquisition system. The signal conditioner separated and amplified the AC and DC components for each channel. The four output signals were then passed to an Alpha 434 Midwestern FM tape recorder. The AC signals were simultaneously recorded on a Brush 220 strip chart recorder and displayed on a Telequipment Oscilloscope (type D67). The DC level was continually monitored by a Fluke 8000A digital multimeter. Readings were taken for a period of five minutes at several heights along the column.

Figure 4 shows typical traces obtained for $d_p = 1.56$ mm at $\epsilon = 0.459$ ($u/u_{mf} = 1.5$) at several heights above the distributor. The dual traces at each height correspond to the simultaneous outputs of the two photodiodes. The top trace corresponds to the signal for the top photodiode. All traces were recorded at a chart speed of 10 mm/s. At 10.16 cm above the distributor, the quasi-periodic signal corresponding to coherent, horizontal traveling voidage waves is clearly demonstrated. The slight lag between the two signals can be seen. At 20.32 cm above the

Table 3. Comparison of experimental and predicted values of the exponent n and the terminal velocity u_t

	Experimental			*From single-sphere correlations*			
Set	n	u_t (extrapolated) (cm/s)	Re_t	n (extrapolated u_t)	u_t (cm/s)	Re_t	n
A	2.87	12.5	73.6	2.89	14.6	86	2.85
B	2.65	15.5	129	2.74	20.7	172	2.66
C	2.44	16.5	158	2.68	27.2	298	2.52
D	2.34	25.7	401	2.44	37.7	588	2.39

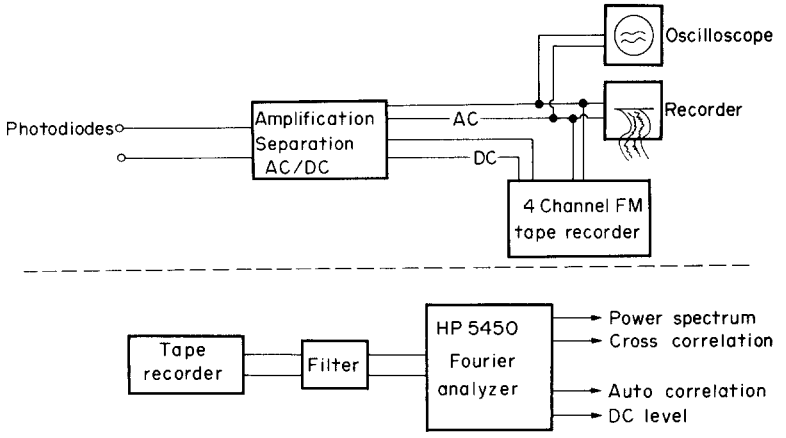

Figure 3. Signal processing flow chart.

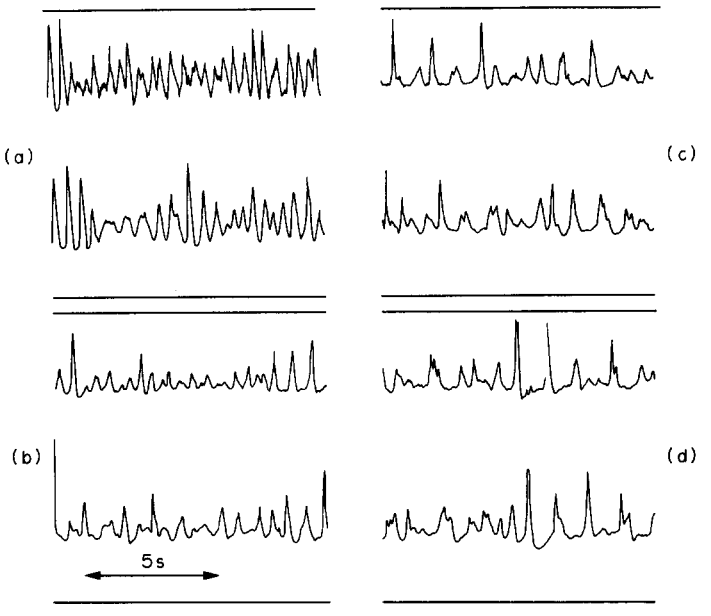

Figure 4. Sample traces for $d_p = 1.56$ mm at $u/u_{mf} = 1.5$. (a) $h = 5.08$ cm; (b) $h = 10.16$ cm; (c) $h = 20.32$ cm; (d) $h = 40.64$ cm.

distributor a distinct, though less periodic signal is still manifested indicating a change in the structure of the waves as they tranverse the diodes. Traces at higher heights are indicative of coalescence and breakup. For instance, at 40.64 cm, an occasional burst in the signal occurs, indicating higher amplitude disturbances. The traces from the top and bottom diodes, though similar, show less periodicity as the bed height is tranversed. The same behavior is encountered at 60.96 cm although the "burst" amplitude seems larger indicating a larger amplitude signal probably due to more frequent cluster formation and coalescence.

The tapes were played back at "real-time" and logged into a model 5450A Hewlett–Packard Fourier Analyzer for processing. Averaging programs were written to give auto power spectrum, auto-correlation, cross-correlation and DC level results for each of the records. The Analyzer was programmed to sample the tape continuously and average several samples of each record. The number of averages depended on the type of function to be computed. Thirty to forty averages were found sufficient for a statistically significant measure on the properties of the AC signal, but only 10–15 records were necessary to obtain the DC level for each run. The term "statistically significant" is used here to mean that a property such as the power spectrum, when

averaged a certain number of times, would yield traces that do not change, either in shape or in magnitude, with further averaging. The records were found to contain no significant frequency components above 25 Hz. In order to avoid aliasing errors a Krohn–Hite model 3323R digital filter was used to eliminate any frequency components from the signal above 20 Hz before inputting to the analyzer. The sampling window contained 512 points. The frequency and amplitude of the dominant component, the mean square value of the averaged time record as well as the time delay between the time records from the two photodiodes were determined accurately. The frequency resolution was 0.09766 Hz whereas the time interval was 20 msec.

The averaged cross-correlation of the two signals obtained from both photodiodes placed 3.5 cm apart gave the time delay required to calculate the velocity of propagation of the waves. Figure 5 shows typical cross-correlation plots obtained. Note the distinctive peak occurring at the time lag required for velocity measurement. From the auto-correlation function, the r.m.s. amplitude of the averaged records could be obtained. Figure 6 gives sample plots of this function. The r.m.s. value of the signal corresponds to the value of the auto-correlation function at zero delay time. We are thus able to obtain the amplitude of the traveling wave disturbances in the bed as a function of height along the column. The averaged power spectrum, a typical sample of which is presented in figure 7, yielded the frequency contact of the signal at all heights studied. Almost all plots showed a dominant frequency component which could be easily determined. The averaged DC level was obtained by taking the Fourier transform of each time record and

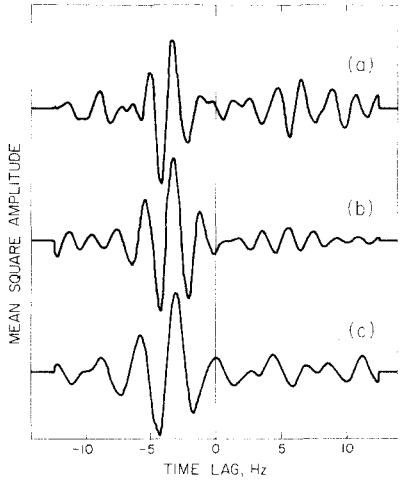

Figure 5. Typical cross-correlation functions $\epsilon = 0.44$, $u/u_{mf} = 1.71$, $d_p = 0.83$ cm. Curves are for 5.08 cm, 10.16 cm and 25.40 cm above the distributor.

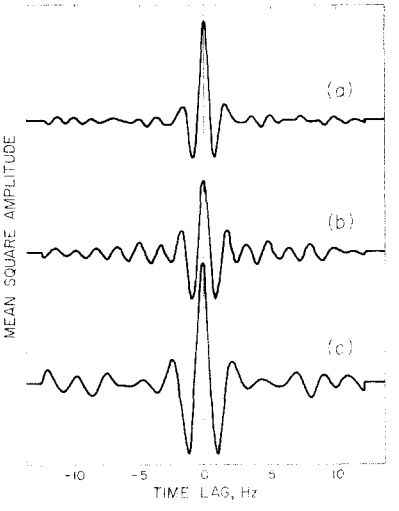

Figure 6. Typical auto-correlation functions. The conditions are the same as for figure 5.

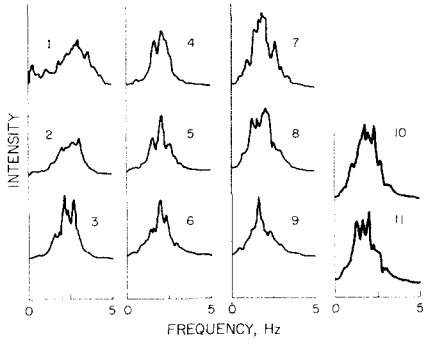

Figure 7. Typical power spectra. The conditions are the same as for figure 5. Curves 1–11 correspond to heights of 5.08 cm, 10.16 cm, 15.24, . . . above the distributor.

averaging in the frequency domain. This was used to relate local disturbance amplitudes to voidage units.

It is important to measure the possible DC variation along the bed length at different flow rates for each bead system under investigation before relating the voltages to voidage units. This was accomplished by performing separate runs described below before changing beads. The DC level, averaged over 1 min varied by at most 1%, and was taken as the DC level corresponding to that particular mean voidage. The value so obtained was virtually independent of heights along the column, indicating the homogeneity of both the Plexiglás walls and the mean voidage.

The plots of DC voltage vs ϵ were straight lines passing through the origin indicating that a simple linear transformation was necessary to translate voltages into voidage units. (In contrast to the more commonly used photomultiplier, the photodiode is a linear transducer, which leads to significant simplifications in the data analysis.)

5. RESULTS

Quantitative measures of the amplitude, velocity of propagation, and dominant frequency were obtained for a range of flow rates as a function of height above the distributor. The dominant frequency, corresponding to the peak in the spectral density, was obtained directly as a digital readout from the HP-5450. The velocity of propagation could be calculated from the time lag for the maximum in the cross-correlation. Two measures of the amplitude could be obtained. The first, from the auto-correlation function at zero time lag, gives the amplitude of the total signal, which we denote as η. The second measure, obtained from the value of the spectral density at its peak, is the amplitude of the dominant wave, denoted as η_d. The discussion here is for the total amplitude η. The behavior for η_d is quite similar and is given by El-Kaissy (1975).

Quantitatively, it was found that the amplitude of the disturbance could be reproduced to within 3% if the wave was coherent and was not going through a stage of coalescence or breakup at the point of measurement. However, if the waves did break up, generally random behavior seemed to take place and the results were only reproducible to within 10%.

The frequency of the dominant component could be reproduced to within 0.09766 Hz. Due to the double-peaked power spectral curves obtained in certain cases at some heights, f_{max} had two values. The lower value always predominated at larger heights, thus leading to a discontinuity in cases where the shift in f_{max} was not smooth.

Measuring the velocity of propagation required a great deal of care due to the sensitivity of this type of measurement to the distance between the photodiodes as well as the delay time obtained from the cross-correlation function. The error in reproducibility varied between 2–6% for all sets of data.

The discussion which follows will consider each set of data separately. The main results as well as the important overall features obtained are given in section 6.

Set A: (figures 8–10)

The amplitude *vs* height is shown for three different flow rates. It should be noted that the data taken were for a narrow range of voidages (0.40–0.427) where the waves appeared to remain coherent for a substantial distance up the bed.

For the smallest voidage, the amplitude increases exponentially. No sign of equilibration or change in the trend is apparent. As the mean voidage is increased an initial exponential growth seems rather evident to a distance of about 20 cm. A "break" in the growth curve appears for a short distance after which an exponential growth with a substantially smaller slopes is manifested. For $\epsilon = 0.422$ two such regions are detected, one for $h = 20$–40 cm and the other for $h = 50$–80 cm. For $\epsilon = 0.427$ only one such break-reform process occurs for $h = 30$–70 cm.

The plot of the frequency of the dominant component versus height indicates a monotonic decrease, asymptotically reaching a limit. Such a limit varies for different flow rates. The trend seems to be a higher limit as flow rate increases.

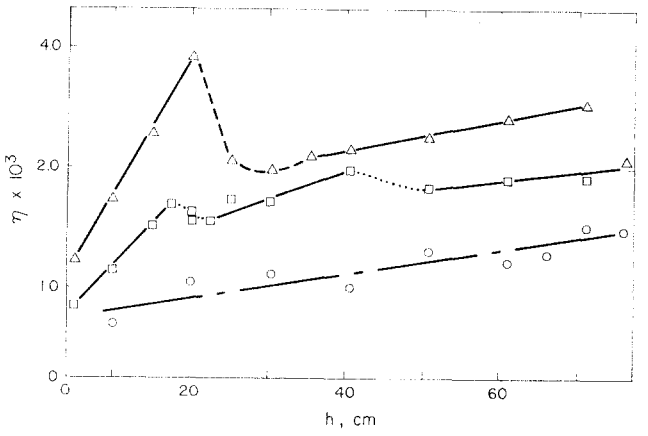

Figure 8. Total amplitude for set A.

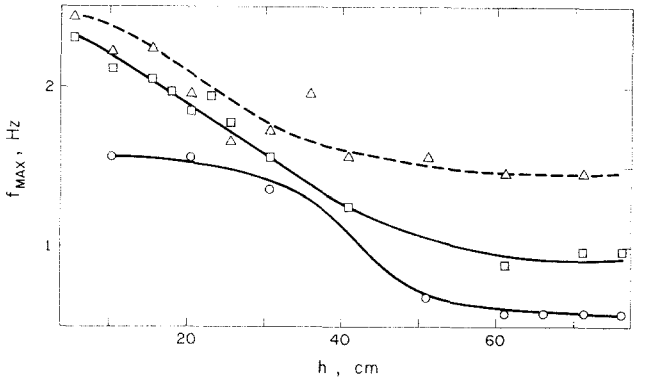

Figure 9. Dominant frequency for set A.

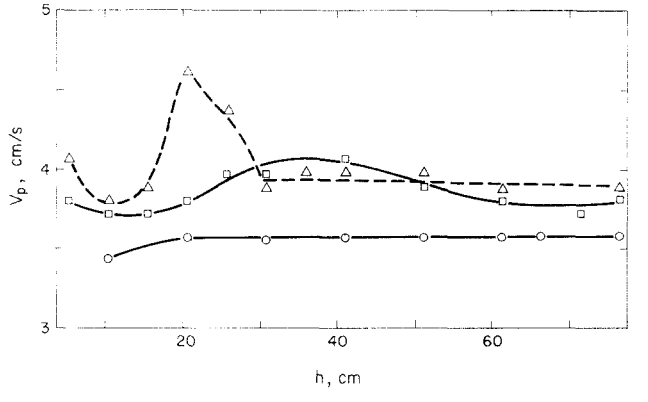

Figure 10. Velocity of propagation for set A.

An initially peculiar behavior in the velocity of propagation is manifested, but the plots indicate that the waves propagate with an increasing velocity, reaching a limit as the top surface of the bed is approached.

It is of interest to investigate the mechanism by which waves grow and coalesce in the bed. We can infer such a behavior from the power spectrum plots obtained in the analysis.

For $\epsilon = 0.401$ the spectrum is wide and peaks as the bed is traversed. The peak becomes pronounced at $h = 30$ cm. A second minor peak appears at a lower frequency. This latter peak grows and overtakes the original one. The peak is well-developed by 50 cm and remains that way for the remaining portion of the bed. As the flow rate is increased to yield $\epsilon = 0.422$, a wide

distribution of frequencies ranging from 0–15 Hz at $h = 5$ cm is evident. As the wave structure develops as it moves up the bed, the spectrum shows a peaking tendency, and a dominant component appears at about 25 cm. Another component of lower frequency appears and overtakes the original one at about 55 cm.

For $\epsilon = 0.427$ quite the same initial behavior is recorded but after the dominant component has developed at about 25 cm a new spread in the distribution appears indicating a breakup of waves. The distribution appears to become organized once more at about $h = 35$ cm, at which point a new dominant component of lower frequency appears and remains for the rest of the region up the bed. The fact that in some cases a double-peaked spectral distribution appears indicates a break-down in coherence and two-dimensionality of the wave train. In most cases, this is coincident with the breaks in the amplitude curves.

Set B: (figures 11–13)

The amplitude versus height for this set of data is studied for a narrow range of voidages ($\epsilon = 0.410$–0.441). For the smallest voidage, the growth of the disturbance is again exponential.

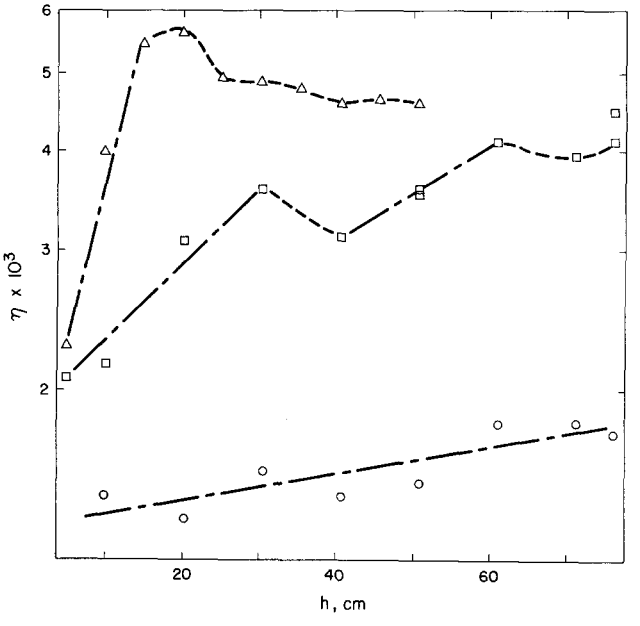

Figure 11. Total amplitude for set B.

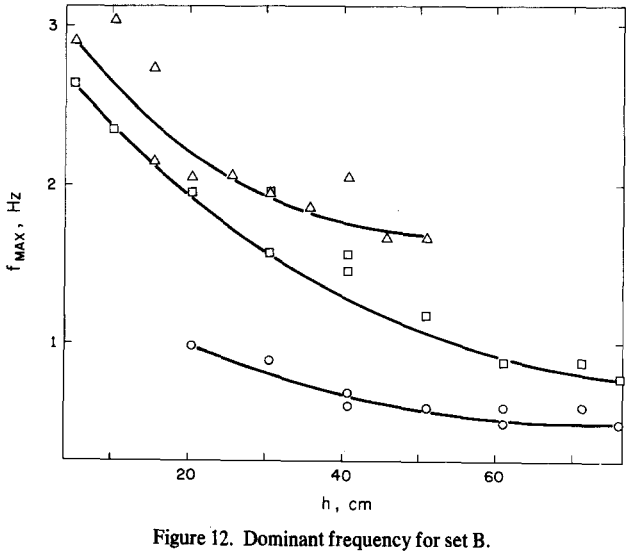

Figure 12. Dominant frequency for set B.

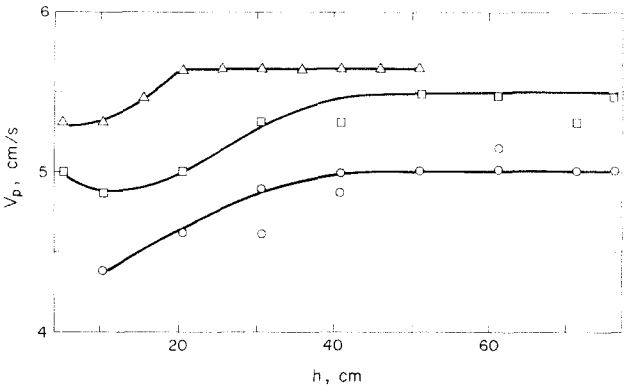

Figure 13. Velocity of propagation for set B.

As the flow rate is increased, an initial exponential growth is manifested. For the case $\epsilon = 0.425$ the initial growth is sustained up to $h = 30$ cm followed by a break-reform phenomenon for $h = 40$–60 cm. The growth rate for the reformed portion is smaller than in the case of initial growth. It appears that an equilibration in amplitude starts to take place thereafter. This is more strongly demonstrated at $\epsilon = 0.441$. The initial exponential growth occurs with a higher growth rate and through a shorter distance. Rebirth of the disturbance does not seem to occur and equilibration of the amplitude takes place over a large portion of the column.

The plot of the frequency of the dominant component component shows the familiar monotonic decay to an asymptotic value. The limit generally increases with increasing flow rate. The velocity of propagation of the disturbance increased rapidly with height for all flow rates. A limiting value was reached as the surface of the bed was approached. Again, the higher the flow rate, the higher the limit.

The change in the power spectrum of the signals at every height for all flow rates studied was recorded. For the smallest flow rate the power spectrum shows the existence of a wide distribution of frequencies up to $h = 10$ cm. A dominant component appears and persists for the remaining portion of the bed but moves slowly to lower frequencies. At a higher flow rate, $\epsilon = 0.425$, very similar behavior is observed, namely, wide distribution close to the distributor followed by the appearance of a characteristic peak at $h = 40$ cm. Another peak at a lower frequency exists which grows with height and eventually overtakes the original peak. No significant change takes place for the remaining length of the bed.

When $\epsilon = 0.441$ an interesting anomaly appears, namely that of a broad but peaked distribution. Close to the distributor no specific well-defined peak is evident but at higher heights peaking manifests itself, though the distribution remains broad compared to those at smaller flow rates. At $h = 20$ cm a lower frequency peak appears. The distribution broadens thereafter with little or no characteristic peak.

Set C: (figures 14–16)

As the bead size is increased the disturbance amplitude increases significantly as can be seen by comparing the ordinates of the amplitude plots for different sets of data.

The initial exponential growth is obtained for this set at all flow rates studied. Equilibration of amplitude is clearly evident from the amplitude plot. Again for this set, the study was carried out at a narrow voidage range. It should be noted that almost identical growth rates are obtained from the two highest flow rates, attributable to the small variation in mean voidage for the two runs.

The plot of the frequency of the dominant component shows the same trend of monotonic decreases to a limit as the waves traverse the column length. The velocity of propagation increases for a considerable portion of the bed length reaching asymptotic limits close to the bed top surface.

For $\epsilon = 0.45$ the power spectrum shows broad distribution close to the distributor after which

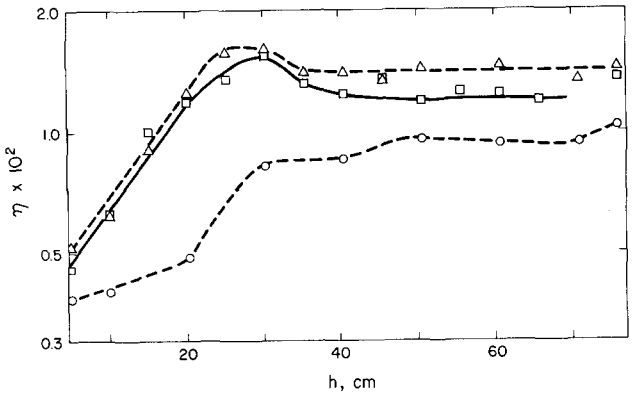

Figure 14. Total amplitude for set C.

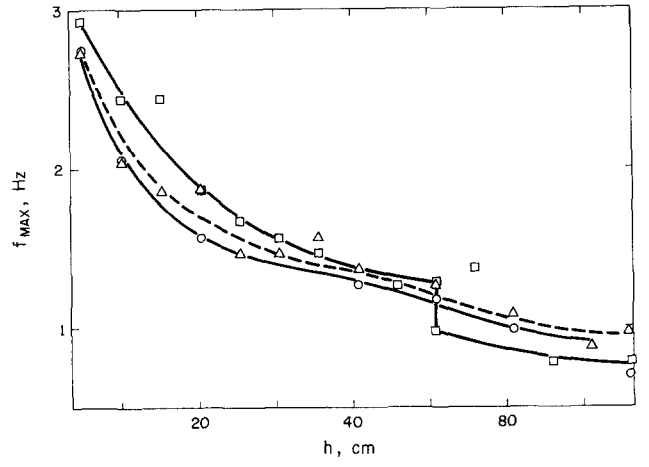

Figure 15. Dominant frequency for set C.

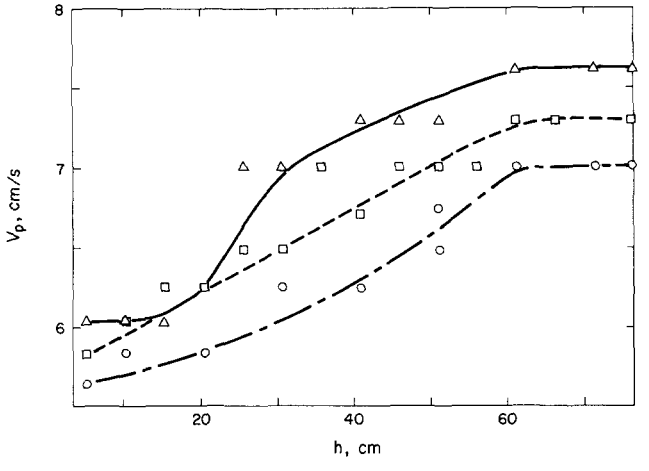

Figure 16. Velocity of propagation for set C.

peaking appears throughout the column. The peak moves to lower frequency rather smoothly.

As the flow rate is increased to $\epsilon = 0.456$ the broad distribution emerges. At $h = 20$ cm a new peak appears at lower frequency that grows and eventually overtakes the original peak. The power spectrum remain peaked thereafter with little frequency change in its dominant component.

At $\epsilon = 0.461$, a peaked but broad distribution at the base appears which remains so up to $h = 25$ cm after which the smaller frequency peak starts appearing. The dominant component shifts to this lower frequency shortly thereafter.

Set D: (figures 17–19)

This was the largest sized beads studied. The amplitude obtained for this set was the largest encountered.

At the lowest flow rate, we observe the characteristic monotonic growth. At $\epsilon = 0.459$ and 0.473 the initial exponential growth is manifested, although for the larger flow rate case the growth rate is considerably larger. The disturbances tend asymptotically to an equilibrium amplitude. The frequency of the dominant component shows the familiar monotonic decrease to a limit. In the use of the highest flow rate studied, data were only taken up to $h = 35$ cm, thus the approached limit could not be determined experimentally.

The velocity of propagation for this bead size increased continuously for $\epsilon = 0.443$ showing no tendency to level to a limit within the range of our data. At higher flow rates a sharp increase to a limit is reached. This limit increases with increasing flow rate.

Looking at the excursions of the power spectrum plots, one observes that for $\epsilon = 0.443$ a broad nonpeaked distribution at the base appears. This distribution starts peaking at $h \sim 10$ cm above the distributor. A new component at lower frequency appears at $h \approx 35$ cm and tends to swamp the higher frequency peak later as it develops. The distribution becomes broad at $h \approx 40$ cm after which a new dominant component emerges. At the two higher flow rates corresponding to $\epsilon = 0.459$ and 0.473 respectively the same behavior is encountered except that the distribution remains broad after the lower and higher frequency peaks have merged.

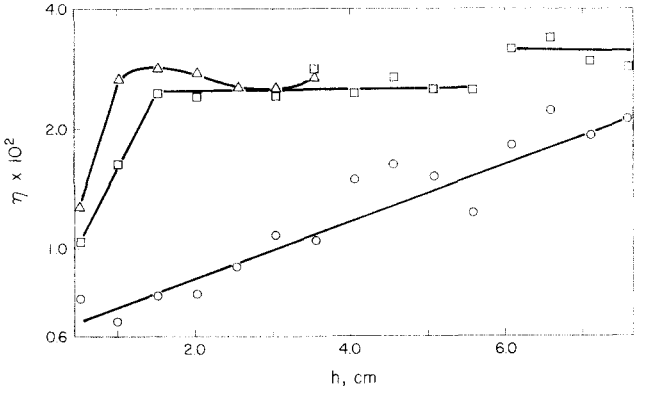

Figure 17. Total amplitude for set D.

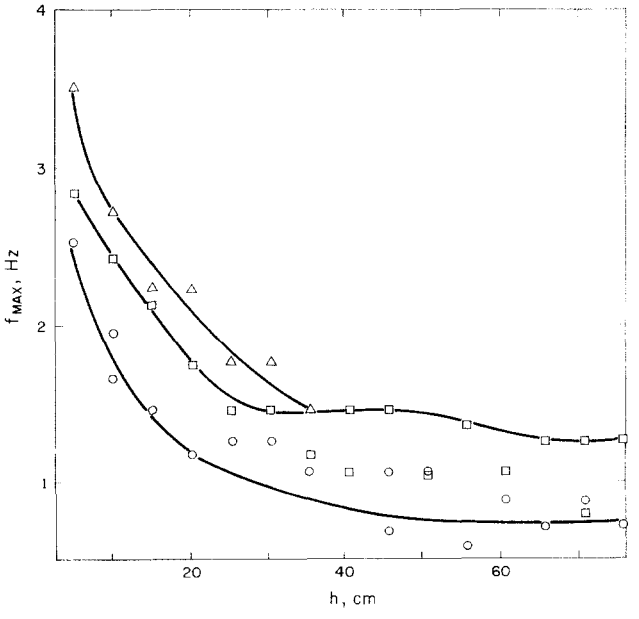

Figure 18. Dominant frequency for set D.

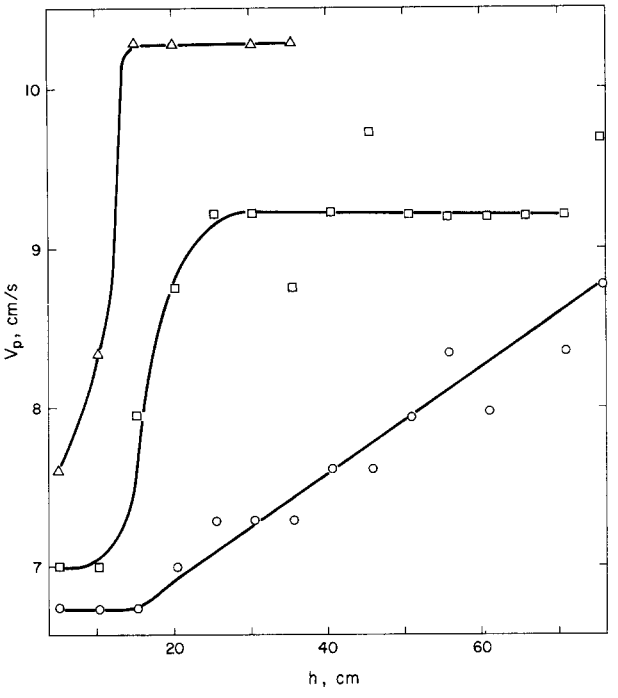

Figure 19. Velocity of propagation for set D.

6. DISCUSSION

In the initial stages of growth, the wave grows exponentially with height with a growth rate which is a function of flow rate and bead size. This is in accord with the qualitative predictions of linear instability theory, although the data indicate that the dominant frequency and propagation velocity vary somewhat during this growth process. Looking ahead to possible comparisons with an instability theory for the inital growth stages, we have recorded the values of the slopes of the straight-line portions of the amplitude plots and these are given as dimensional growth constants in table 4.

Loss of coherence and attenuation of amplitude is either followed by another region of exponential growth or is accompanied by the dramatic pinching off of the wave to form circular structures, strongly suggesting that bubbles can and do form from instability waves. At the point at which break-up occurs, the qualitative measurements must be interpreted in a statistical sense, since the motions are no longer ordered, "laminar" states. The surprising indications are that for

Table 4. The experimental growth constants for both the total disturbance and the dominant wave

Run	σ (cm^{-1})	σ_d (cm^{-1})
A1	0.0068	0.013
A2	0.046	0.075
A3	0.075	0.12
B1	—	0.012
B2	0.022	0.048
B3	0.095	0.12
C1	0.017	0.045
C2	0.060	0.067
C3	0.060	0.067
D1	0.023	—
D2	0.089	0.13
D3	0.15	0.21

a given bead size and flow rate, the expected values of the amplitude, velocity of propagation, and dominant frequency approach equilibrated values. Perhaps even more surprising, the equilibrated amplitude appears to be independent of flow rate. This amplitude increases dramatically with particle size, while the other propagation properties vary over much smaller ranges.

Elementary dimensional analysis predicts that any property of the fluid-mechanical state, made dimensionless using $\{ud_p\}$ as velocity and length scales, should be a function of at most five independent dimensionless groups:

$$Re = \frac{ud_p}{\nu} \quad \text{the particle Reynolds number,}$$

$$Fr = \frac{u^2}{gd_p} \quad \text{the particle Froude number,}$$

ρ_s/ρ_f the density ratio,

$L/d_p, D/d_p$ bed size, measured in particle diameters.

Of these, onle Re and Fr could be varied independently in the present experiments. ρ_s/ρ_f was fixed at approximately 4, and both L/d_p and D/d_p were in most cases substantially greater than 15, which is commonly thought to be effectively infinite as far as wall effects are concerned. Thus Re, Fr are the only independent groups remaining. The actual choice of these two is of course arbitrary. Furthermore, given the drag relation, e.g. the Richardson–Zaki correlation, u_{mf} is determined implicitly by a relation between ϵ_{mf}, Re_{mf}, Fr_{mf} and ρ_s/ρ_f. Thus we may find it advantageous to utilize "secondary" scaling parameters such as u_{mf} and ϵ_{mf} in an attempt to discover scaling laws for the expected values of certain statistically defined properties of the late stage developed structures occurring in the region of equilibration. Three such properties were measured in this study; the expected values for half peak-to-peak amplitude, velocity of propagation and the dominant frequency of the events which visual observations indicate correspond to the formation and propagation of bubble-like clusters. These expected values are given in table 5 as a function of Re, Fr, Re^2/Fr, and u/u_{mf} for those runs in which the data in figures 8–19 indicate equilibration.

We consider that the present data are limited and fairly sparse, so that their extrapolation or the development of scaling laws from them is premature, and more extensive data are required especially for varying ρ_s/ρ_f, before such attempts should be made. Below, however, is our preliminary thinking on possible important scale parameters.

As we have noted, the amplitude seems to equilibrate at a value independent of flow rate. Thus we might expect it to scale with $Re^2/Fr = gd_p^3/\nu^2$. Table 5 indicates that this is indeed the case, with the expected amplitude increasing with increasing Re^2/Fr. Particle size thus has a strong effect, with amplitude increasing roughly as the cube of the particle diameter. If this

Table 5. Expected values of amplitude, frequency and velocity of equilibrated structures

Run	η	$f^* = f_{max} d_p/u$	$v^* = V_p/u$	Re	Fr	$Re^2/Fr \times 10^{-4}$	u/u_{mf}
A1	↑	0.0222	3.8	5.61	0.0157		1.49
A2	2×10^{-3}	0.054	3.7	6.1	0.0188	2.0	1.63
A3	↓	0.0775	3.5	6.6	0.0216		1.75
B1	↑	0.028	3.7	12.4	0.0272		1.37
B2	4.5×10^{-3}	0.037	3.3	14.0	0.035	5.6	1.54
B3	↓	0.076	3.0	15.5	0.0425		1.71
C1	↑	0·038	2.7	28.6	0.0633		1.37
C2	1.4×10^{-2}	0.037	2.7	29.4	0.0670	13.	1.41
C3	↓	0.036	2.7	30.2	0.0708		1.45
D1	↑	0.0314	—	58.1	0.091		1.36
D2	2.7×10^{-2}	0.067	2.5	63.9	0.109	36.	1.49
D3	↓	—	2.0	69.8	0.131		1.63

interpretation is correct, it implies that initial growth rates may be relatively *unimportant* in determining the ultimate structure of a fluidized bed.

The data in table 4 seem to support the idea that the velocity of propagation, scaled by u, is relatively constant, although there is a weak particle size effect. On the other hand, the dimensionless dominant frequency seems to correlate strongly with u/u_{mf}, and hence to some complicated combination of Re, Fr, ρ_s/ρ_f since u_{mf} is implicitly related to these groups.

In conclusion, we have presented the first statistically significant measurements of the propagation properties of voidage waves in fluidized beds and have shown conclusively that the breakup of these waves is followed by a mode of motion suggestive of bubble formation. The quantitative results will be compared with linear instability predictions in a subsequent paper.

Acknowledgement—Acknowledgement is made to the donors to the Petroleum Research Fund, administered by the American Chemical Society, for partial support of this research. The financial support of the National Science Foundation through Grant GK-27902 is also gratefully acknowledged. Mr. Ben Mohilef rendered invaluable aid in the design and construction of the photo-optical package.

REFERENCES

ANDERSON, T. B. & JACKSON, R. 1968 A fluid mechanical description of fluidized beds—stability of the state of uniform fluidization. *I/EC Fundamentals* **7**, 12–21.

ANDERSON, R. B. & JACKSON, R. 1969 A fluid mechanical description of fluidized beds—comparison of theory and experiment. *I/EC Fundamentals* **8**, 137–144.

CLIFT, R. & GRACE, J. R. 1972 The mechanism of bubble break-up in fluidized beds. *Chem. Engng Sci.* **27**, 2309–2310.

DAVIDSON, J. F. & HARRISON, D. 1963 *Fluidized Particles.* Cambridge University Press, London.

EL-KAISSY, M. M. 1975 The thermomechanics of multiphase systems with application to fluidized continua. Ph.D. Thesis, Stanford University.

HASSET, N. J. 1961 Flow patterns in particle beds. *Nature, Lond.* **189**, 997–998.

HASSET, N. J. 1961 The mechanism of fluidization. *Br. Chem. Engng* **6**, 777–780.

HIBY, J. W. 1967 Periodic phenomena connected with gas–solid fluidization. *Proc. Int. Symp. on Fluidization* (Drinkenburg, A. Ed.). Netherlands University Press.

JACKSON, R. 1963 The mechanics of fluidized beds: Part 1: The stability of the state of uniform fluidization, *Trans. Instn Chem. Engrs* **41**, 13–21.

JACKSON, R. 1971 Fluid mechanical theory. *Fluidization* (Davidson, J. F. and Harrison, D. Eds.). Academic Press, New York.

JONES, B. R. E. & PYLE, D. L. 1971 On stability, dynamics and bubbling in fluidized beds. *Chem. Engng Prog. Symp. Ser.* No. 116, **67**, 1–10.

LAWSON, A. & HASSET, N. J. 1967 Discontinuities and flow patterns in liquid–fluidized beds. *Proc. Int. Symp. on Fluidization* (Drinkenburg, A. Ed.), Netherlands University Press, Eindhoven, Nd.

MEDLIN, J. *et al.* 1974 Fluid mechanical description of fluidized beds—convective instabilities in bounded beds. *I/EC Fundamentals* **13**, 247–258.

ROWE, P. N. 1971 Experimental properties of bubbles. *Fluidization* (Davidson, J. F. and Harrison, D. Eds.). Academic Press, New York.

VERLOOP, J. & HEERTJES, P. M. 1974 On the origin of bubbles in gas-fluidized beds. *Chem. Engng Sci.* **29**, 1101–1107.

WERTHER, J. & MOLERUS, O. 1973 The local structure of gas fluidized beds. 1. A statistically based measuring system. *Int. J. Multiphase Flow* **1**, 103–122.

WILHELM, R. H. & KWAUK, M. 1948 Fluidization of solid particles, *Chem. Engng Prog.* **44**, 201–218.

ZENZ, F. 1971 Regimes of fluidized behavior. *Fluidization* (Davidson, J. F. and Harrison, D. Eds.). Academic Press, New York.